ACS APPLIED MATERIALS & INTERFACES

Research Article

www.acsami.org

A Novel Cobalt-Free, CO_2-Stable, and Reduction-Tolerant Dual-Phase Oxygen-Permeable Membrane

Zhongtao Wang,[†] Wenping Sun,[†] Zhiwen Zhu,[†] Tong Liu,[†] and Wei Liu*[,†,‡]

[†]CAS Key Laboratory of Materials for Energy Conversion, Department of Materials Science and Engineering, University of Science and Technology of China, Hefei 230026, China

[‡]Key Laboratory of Materials Physics, Institute of Solid State Physics, Chinese Academy of Sciences, Hefei 230031, China

ABSTRACT: A novel CO_2-stable and reduction-tolerant $Ce_{0.8}Sm_{0.2}O_{2-\delta}$–$La_{0.9}Sr_{0.1}FeO_{3-\delta}$ (SDC–LSF) dense dual-phase oxygen-permeable membrane was designed and evaluated in this work. Homogeneous SDC–LSF composite powders for membrane fabrication were synthesized via a one-pot combustion method. The chemical compatibility and ion interdiffusion behavior between the fluorite phase SDC and perovskite phase LSF during the synthesis process was studied. The oxygen permeation flux through the dense dual-phase composite membranes was evaluated and found to be highly dependent on the volume ratio of SDC and LSF. The SDC–LSF membrane with a volume ratio of 7:3 (SDC70–LSF30) possessed the highest permeation flux, achieving 6.42 × 10^{-7} mol·cm^{-2}·s^{-1} under an air/CO gradient at 900 °C for a 1.1-mm-thick membrane. Especially, the membrane performance showed excellent durability and operated stably without any degradation at 900 °C for 450 h with helium, CO_2, or CO as the sweep gas. The present results demonstrate that a SDC70–LSF30 dual-phase membrane is a promising chemically stable device for oxygen production and CO_2 capture with sufficiently high oxygen permeation flux.

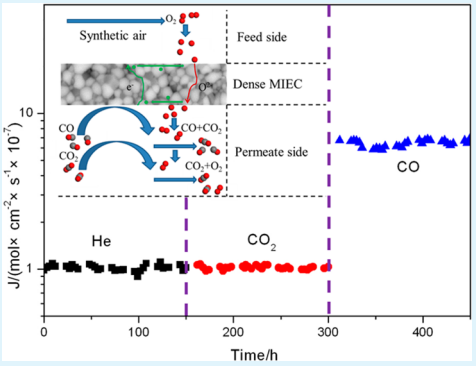

KEYWORDS: *oxygen permeation, CO_2-stable membrane, reduction-tolerant membrane, stability, dual-phase membrane*

1. INTRODUCTION

Dense oxygen permeation membranes with mixed ionic–electronic conducting (MIEC) ability are attracting ever-increasing attention because of their potential applications in producing pure oxygen from air,[1,2] partial oxidation of methane to syngas,[3−5] and oxyfuel combustion for CO_2 capture[6,7] and some other applications as membrane reactors.[8,9] Traditional oxygen permeation membranes are usually made of typical perovskite-type oxides, such as $La_{0.6}Sr_{0.4}Co_{0.8}Fe_{0.2}O_{3-\delta}$,[10] $Ba_{0.5}Sr_{0.5}Co_{0.8}Fe_{0.2}O_{3-\delta}$,[11,12] and $SrCo_{0.8}Fe_{0.2}O_{3-\delta}$.[13,14] These materials generally show high oxygen permeation ability; however, the poor chemical and structure stability under CO_2- or SO_2-containing atmospheres or atmospheres with a low oxygen partial pressure[10,12,15] hampers their widespread applications.

Recently, dual-phase membranes consisting of oxygen ionic and electronic conducting phases were widely studied because of their good stability and relatively high performance.[1] Perovskite-type oxides exhibit high p-type electronic conductivity under oxygen permeation conditions and are good candidates as electronic conducting phases. $La_{0.8}Sr_{0.2}(Cr,Mn)O_{3-\delta}$,[16−18] $La_{0.8}Sr_{0.2}Cr_{0.5}Fe_{0.5}O_{3-\delta}$,[19,20] and some other MIEC oxides, such as $RBaCoO_{5+\delta}$ (R = La, Pr, Gd),[21−23] $(Sm,Pr)_{0.6}Sr_{0.4}FeO_{3-\delta}$,[24−26] and $Sm_{1-x}Ca_xMn_{0.5}Co_{0.5}O_{3-\delta}$,[27] were systematically investigated as electronic conducting phases and showed promising oxygen permeation performance. Wang et al. reported that the oxygen permeation flux through a 0.3-mm-thick $Ce_{0.8}Sm_{0.2}O_{2-\delta}$ (SDC)–$La_{0.8}Sr_{0.2}CrO_{3-\delta}$ dual-phase membrane reached 8.6 × 10^{-7} mol·cm^{-2}·s^{-1} at 950 °C, and no flux degradation was observed within a period of 110 h.[17] The oxygen permeation flux through a 0.6-mm-thick SDC–$LaBaCo_2O_{5+\delta}$ membrane under an air/helium gradient achieved 4.59 × 10^{-7} mol·cm^{-2}·s^{-1} at 950 °C.[21] However, it should also be noted that most of the perovskite-type electronic conducting materials contain cobalt or chromium. Generally, cobalt-containing perovskite oxides have large linear expansion coefficients that can lead to structural instability, eventually introducing microcracks in membranes during thermal cycling. For chromium-containing materials, chromium evaporation easily occurs at elevated temperatures,[28,29] and this would hinder their industrial applications. Apart from those perovskite-type oxides, Fe_2O_3[30] and some spinel oxides[1,31−33] were also developed as electronic conducting phases in the past few years. The corresponding dual-phase oxygen permeation membranes had excellent CO_2 tolerance. For instance, a stable oxygen permeation flux of 3.57 × 10^{-7} mol·cm^{-2}·s^{-1} through a 0.3-mm-thick 40 wt % $Mn_{1.5}Co_{1.5}O_{4-\delta}$–60 wt % $Ce_{0.9}Pr_{0.1}O_{2-\delta}$ membrane was obtained at 1000 °C under an air/CO_2 gradient.[31] The oxygen permeation flux through a $NiFe_2O_4$–$Ce_{0.9}Gd_{0.1}O_{2-\delta}$ dual-phase membrane showed no decline after operating for 100 h using CO_2 as the sweep gas.[1]

Received: August 7, 2013
Accepted: September 30, 2013
Published: September 30, 2013

In this work, cobalt/chromium-free $La_{0.9}Sr_{0.1}FeO_{3-\delta}$ (LSF) was employed as the electronic conducting phase, combined with SDC as the oxygen ionic conducting phase, to construct dual-phase oxygen permeation membranes. Uniform and homogeneous dual-phase membranes were successfully fabricated with nominal SDC−LSF composite powders synthesized via a one-pot combustion method. The oxygen permeation ability and performance stability of the membranes were investigated systematically.

2. EXPERIMENTAL SECTION

2.1. Preparation of Powders and Membranes. $Ce_{0.8}Sm_{0.2}O_{2-\delta}$−$La_{0.9}Sr_{0.1}FeO_{3-\delta}$ (SDC−LSF) dual-phase composite powders with volume ratios of 6:4, 7:3, and 8:2 were synthesized via a one-pot combustion method, as described elsewhere.[25,34] The as-prepared powders were calcined at 1000 °C for 3 h and then pressed to button-shaped disks via a typical uniaxial dry-pressing process. The green disks were sintered at 1400 °C for 5 h in static air. Both surfaces of the sintered disks were carefully polished using a 1000-mesh abrasive paper to obtain SDC−LSF membranes with a thickness of around 1 mm. The three samples with volume ratios of 6:4, 7:3, and 8:2 are hereafter abbreviated to SDC60−LSF40, SDC70−LSF30, and SDC80−LSF20, respectively.

2.2. Characterization of Powders and Membranes. The phase structures of the powders and membranes were examined using X-ray diffraction (XRD; Rigaku TTR-III) with Cu Kα radiation. The surface morphology of the membranes was observed by scanning electron microscopy (SEM; JEOL JSM-6700F). The electrical conductivities were measured using a typical direct-current four-probe technique in the temperature range from 650 to 850 °C. To evaluate the CO_2 tolerance of the composite powders, the powders were treated in dry CO_2 with a flow rate of 40 mL·min^{-1} at 900 °C for 12 h. The chemical composition of SDC and doped CeO_2 in the composite powders was analyzed by inductively coupled plasma atomic emission spectrometry (ICP-AES; Optima 73 00 DV). Before ICP-AES measurement, the SDC−LSF composite powders were etched in 2 M HNO_3 to dissolve the perovskite phase of LSF. Then, the suspension was filtered to obtain the undissolved doped CeO_2 powders. The doped CeO_2 powders were then washed four times with deionized water under stirring followed by ethanol to eliminate the existence of other absorbed metal ions.

2.3. Oxygen Permeation Measurement. The oxygen permeation flux through the dual-phase SDC−LSF membrane was measured in the temperature range of 800−1000 °C. The polished membrane was cleaned in ethanol and then sealed on a Al_2O_3 tube with a glass ring as the sealant. One side of the membrane was exposed to ambient air; the other side was swept by helium or CO_2 with a flow rate of 40 mL·min^{-1} or by CO with a flow rate of 20 mL·min^{-1}. The composition of the permeated effluent gas was determined by gas chromatography (GC1690T, Kexiao, China). The oxygen flux from leakage through the sealant was corrected by determining the dinitrogen concentration in the permeated gas. During the measurement, the sealing efficiency was higher than 95%.

3. RESULT AND DISCUSSION

3.1. Phase Composition. Figure 1 shows the XRD patterns of the nominal SDC−LSF dual-phase composite powders with different volume ratios and the single-phase SDC and LSF powders synthesized via the same route. It is clearly shown that the composite powders are composed of a fluorite phase and a perovskite one, and no other impurity phases are present. Similar results were obtained in other dual-phase composite powders synthesized via the one-pot combustion method, such as SDC−$Sm_{0.6}Sr_{0.4}FeO_{3-\delta}$[35,36] and $Mn_{1.5}Co_{1.5}O_{4-\delta}$−$Ce_{0.9}Pr_{0.1}O_{2-\delta}$.[31] The fluorite phase can be assigned to doped CeO_2, while the perovskite phase should be doped $LaFeO_3$. In the previous reports,[25,27,31,35] ion interdiffusion between the fluorite and perovskite phases was usually ignored. In this work, efforts were made to determine the exact chemical composition of the two phases. Figure 2 shows the XRD patterns of the residual powders after etching the dual-phase composite powders in diluted nitric acid, and the XRD patterns of the SDC powders before and after etching are also displayed for comparison. Obviously, diffraction peaks corresponding to the perovskite phase disappear, and only peaks corresponding to the fluorite phase are present, indicating that doped $LaFeO_3$ is completely dissolved and doped CeO_2

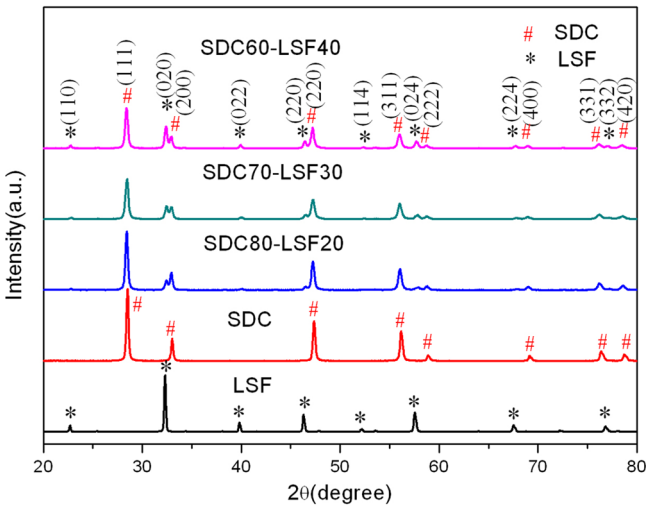

Figure 1. XRD patterns of SDC−LSF composite powders derived from the one-pot combustion process as well as single SDC and LSF powders.

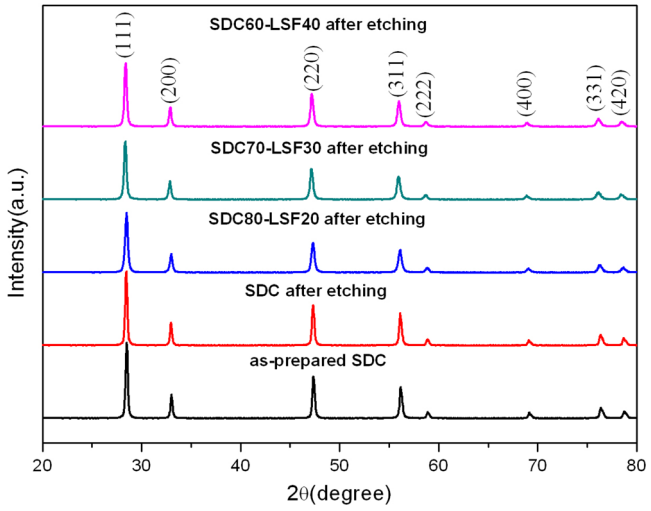

Figure 2. XRD patterns of SDC−LSF composite and SDC powders after etching in 2 M HNO_3 as well as fresh SDC powders.

Table 1. Cell Parameters of Doped CeO_2 in SDC−LSF Composite and Single-Phase SDC Powders

		after etching			
	as-prepared SDC	SDC	SDC60−LSF40	SDC70−LSF30	SDC80−LSF20
a/Å	5.423	5.428	5.448	5.449	5.443
cell volume/Å^3	159.52	159.92	161.71	161.77	161.25

Table 2. Chemical Composition and Estimated Molecular Formula of Doped CeO_2 in SDC−LSF Composite and Single-Phase SDC Powders

		La mol %	Ce mol %	Sm mol %	Fe mol %	Sr mol %	molecular formula
as-prepared	SDC	0	81.31 ± 2.85	18.68 ± 0.52	0	0	$Ce_{0.813}Sm_{0.187}O_{2-\delta}$
after etching	SDC	0	80.62 ± 2.76	19.38 ± 0.61	0	0	$Ce_{0.806}Sm_{0.194}O_{2-\delta}$
	SDC60−LSF40	9.18 ± 0.24	78.34 ± 2.67	12.09 ± 0.30	0.40 ± 0.002	0	$Ce_{0.783}(Sm_{0.121}La_{0.092}Fe_{0.004})O_{2-\delta}$
	SDC70−LSF30	8.76 ± 0.27	77.39 ± 2.70	13.21 ± 0.34	0.7 ± 0.007	0	$Ce_{0.774}(Sm_{0.132}La_{0.087}Fe_{0.007})O_{2-\delta}$
	SDC80−LSF20	8.12 ± 0.18	75.91 ± 2.51	14.64 ± 0.27	1.4 ± 0.010	0	$Ce_{0.759}(Sm_{0.146}La_{0.081}Fe_{0.014})O_{2-\delta}$

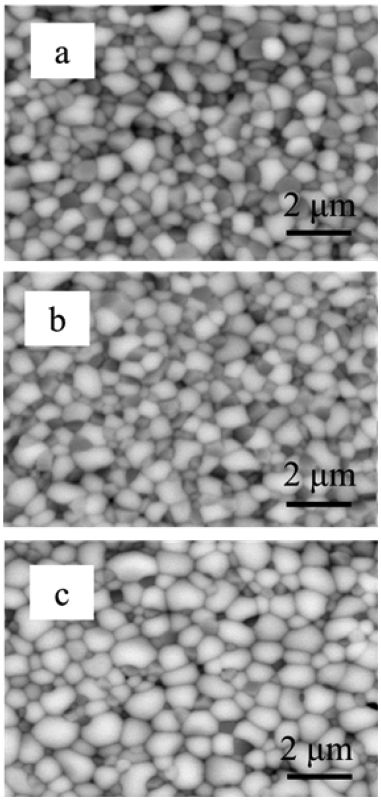

Figure 3. BSEM images of the sintered SDC−LSF dual-phase membranes: SDC60−LSF40 (a); SDC70−LSF30 (b); SDC80−LSF20 (c). The gray grains are LSF, while the white ones are SDC.

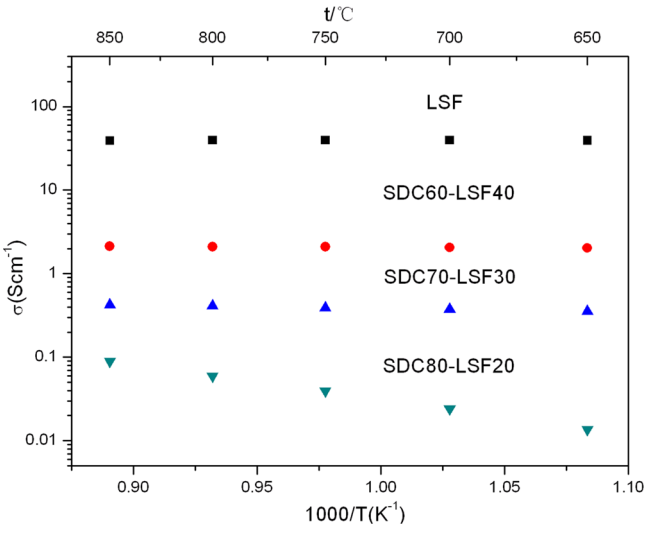

Figure 4. Temperature dependence of the conductivity of the LSF and SDC−LSF samples.

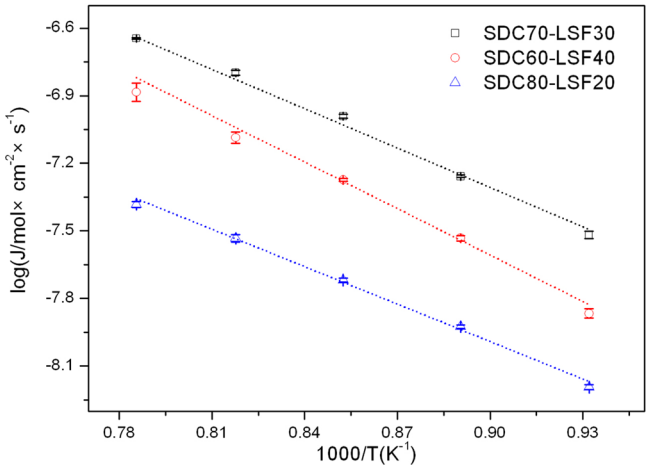

Figure 5. Arrhenius plot of the oxygen permeation flux through SDC−LSF membranes: with helium as the sweep gas at a rate of 40 mL·min^{-1}. Membrane thickness: 1.1 mm.

survives. Besides, one can see that the characteristic peaks of the fluorite phase in the composite powders shift toward lower reflection angles compared to those of the single-phase SDC, suggesting an increase of the cell parameters. The cell parameters of the doped CeO_2 powders are calculated and summarized in Table 1. To further examine the exact chemical composition of the doped CeO_2, ICP-AES measurement of the powders was performed, and the result is displayed in Table 2. It can be found that the doped CeO_2 powders were codoped with Sm^{3+}, La^{3+}, and a minor amount of iron. Because the ionic radius of La^{3+} (0.1160 nm) is larger than that of Sm^{3+} (0.1079 nm) in eight-coordination,[37] the codoped CeO_2 powders would have larger cell parameters, and this is well confirmed by the calculated cell parameters according to the XRD results (Table 1). Moreover, it has been well-proven that codoping is an effective strategy to improve the conductivity of doped CeO_2 oxide ionic conductors.[38−40] Thus, it can be anticipated that this Sm^{3+}- and La^{3+}-codoped CeO_2 phase would be beneficial for enhancing the oxygen permeation ability of the dual-phase membrane.

3.2. Microstructure and Conductivity. Figure 3 shows backscattered SEM (BSEM) images of the surface morphology of the as-sintered nominal SDC−LSF dual-phase membranes. It can be seen that LSF and SDC grains distribute very uniformly in the membranes. In addition, two phases also distribute continuously in the samples except SDC80−LSF20. For SDC80−LSF20, the LSF grains spread like isolated islands in the SDC matrix, which is similar to that reported in the literature,[30] and this configuration is detrimental to the electronic percolation conductivity of the membrane. Figure 4 shows the temperature dependence of the electrical conductivity of SDC−LSF composites and LSF. Obviously, the electrical conductivity of LSF is far higher than that of SDC.

Table 3. Oxygen Permeation Flux ($\times 10^{-7}$ mol·cm^{-2}·s^{-1}) of Some Reported Oxygen-Permeable Membranes with CO_2/Helium as the Sweep Gas

membrane type	thickness (mm)	temperature (°C)	oxygen flux air/helium	oxygen flux air/CO_2	ref
$Ba_{0.5}Sr_{0.5}Co_{0.8}Fe_{0.2}O_{3-\delta}$	1	875	14.14	0	12
$La_{0.9}Sr_{0.1}FeO_{3-\delta}$	1	1000	0.22		48
$Ce_{0.9}Gd_{0.1}O_{2-\delta}$–$NiFe_2O_4$	0.5	950	1.34	1.19	1
$Ce_{0.9}Pr_{0.1}O_{2-\delta}$–$Pr_{0.6}Sr_{0.4}FeO_{3-\delta}$	0.6	950	2.01	1.34	25
$Ce_{0.9}Gd_{0.1}O_{2-\delta}$–$Fe_2O_3$	0.5	950	0.74	0.60	30
SDC70–LSF30	1.1	950	1.59 ± 0.04	1.59 ± 0.03	this work

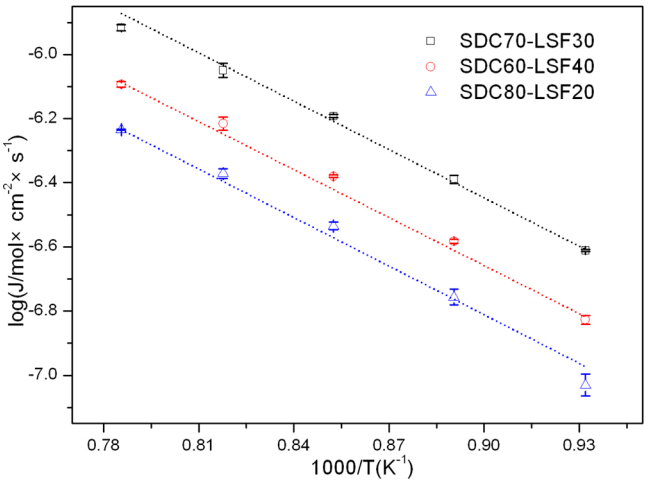

Figure 6. Arrhenius plot of the oxygen permeation flux through SDC–LSF membranes: with CO as the sweep gas at a rate of 20 mL·min^{-1}. Membrane thickness: 1.1 mm.

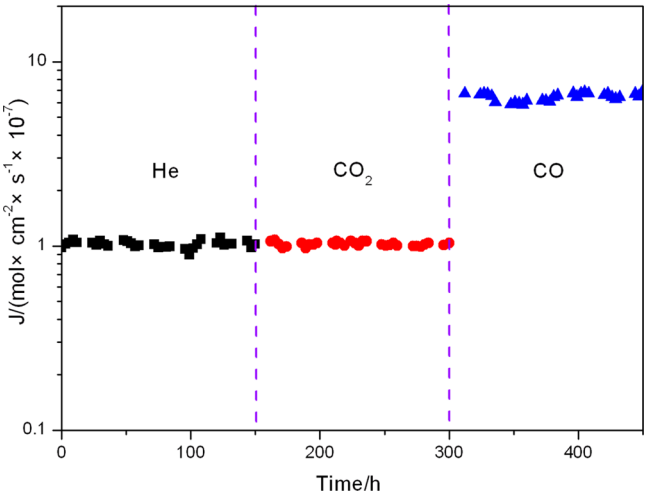

Figure 7. Time dependence of the oxygen permeation flux at 900 °C under air/helium, air/CO_2, and air/CO gradients. Membrane thickness: 1.1 mm.

Thus, the ambipolar conductivity[41] of SDC–LSF should be controlled by the oxygen ionic transport of SDC when LSF can percolate in the dual-phase membrane. The electrical conductivity of SDC80–LSF20 is very close to that of SDC,[42−44] indicating that the LSF phase cannot form a continuous network to provide enough electronic transport, which is consistent with the BSEM results (Figure 3c). For SDC80–LSF20, the oxygen permeation behavior would be limited by both oxygen ionic and electronic transport according to the Wagner equation.[45]

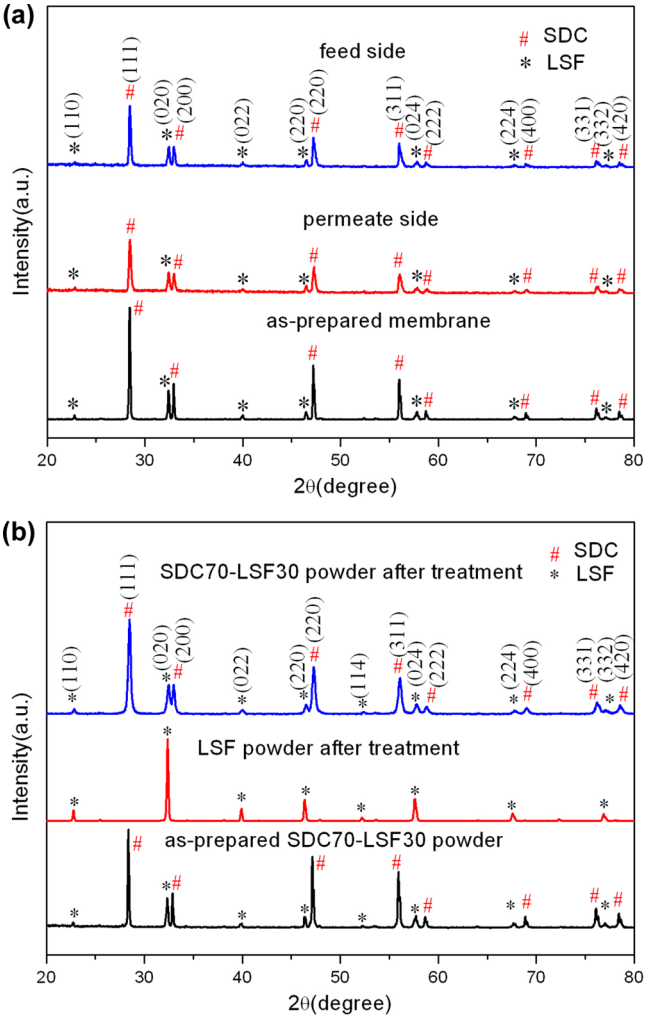

Figure 8. (a) XRD patterns of the SDC70–LSF30 membrane before and after testing. (b) XRD patterns of LSF and SDC70–LSF30 powders annealed in dry CO_2 at 900 °C for 12 h as well as the fresh SDC70–LSF30 powders.

3.3. Oxygen Permeation. Figure 5 shows the oxygen permeation performance of the SDC–LSF membranes with helium as the sweep gas over the temperature range of 800–1000 °C. It can be seen that the oxygen permeation flux increases with the operating temperature. The SDC70–LSF30 membrane shows the highest oxygen permeation flux among the three samples, and the flux reaches 1.59×10^{-7} mol·cm^{-2}·s^{-1} at 950 °C. On the basis of the conductivity results, the electronic conducting phase LSF percolates in SDC60–LSF40 and SDC70–LSF30. As reported in the previous literature,[16,46] the oxygen ionic conductivity of dual-phase composites is much smaller than that of a single-phase SDC ceramic even after

dx.doi.org/10.1021/am403272z | ACS Appl. Mater. Interfaces 2013, 5, 11038−11043

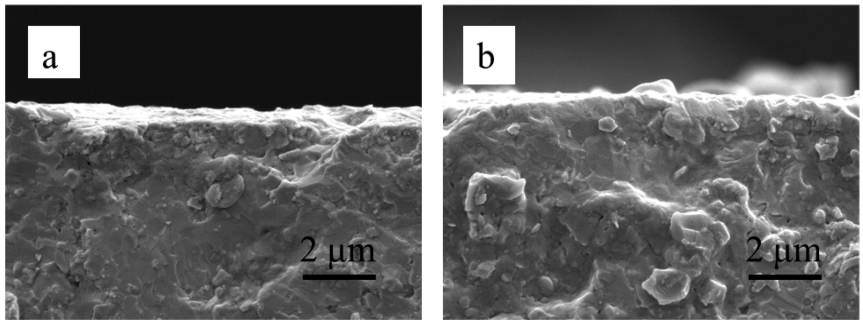

Figure 9. SEM images of the SDC−LSF dual-phase membrane before (a) and after (b) testing.

correction for the volume fraction of the SDC phase in the composites. This could be partly attributed to the blocking of oxygen-ion-transporting paths by the electronic conducting phase. Thus, the oxygen permeation performance increases with increasing SDC content in this case. For SDC80−LSF20, LSF cannot percolate in the membrane, and hence the ambipolar conductivity is limited by the low electronic conductivity. Consequently, this membrane exhibits the lowest oxygen permeation flux. The apparent activation energy (E_a) of the flux was also calculated according to Figure 5. The E_a values are 106.1 ± 4.1, 111.5 ± 3.3, and 131.6 ± 7.2 kJ·mol^{-1} for SDC80−LSF20, SDC70−LSF30, and SDC60−LSF40, respectively. The E_a value is very close to that of some other reported dual-phase membranes, which are 122.6 ± 6.0 kJ·mol^{-1} for SDC−$La_{0.8}Sr_{0.2}CrO_{3-\delta}$[16] and 125 ± 2 kJ·mol^{-1} for $Ce_{0.85}Sm_{0.15}O_{2-\delta}$−$Sm_{0.6}Sr_{0.4}FeO_{3-\delta}$.[26] It has to be noted that the oxygen flux through the 1.1-mm-thick SDC70−LSF30 membrane is comparable and even higher than those of other cobalt-free dual-phase oxygen permeation membranes (around 0.5 mm in thickness), which are much thinner than SDC70−LSF30, as shown in Table 3. According to the Wagner equation,[45] the oxygen permeation flux is inversely proportional to the membrane thickness when oxygen permeation is rate-limited by bulk diffusion. For membranes with thicknesses of around hundreds of micrometers, the oxygen permeation flux is limited by bulk diffusion of oxygen ions.[47] Thus, the permeation flux will double the present value if the thickness of the SDC70−LSF30 membrane is reduced to 0.5 mm and will achieve about 3.5 × 10^{-7} mol·cm^{-2}·s^{-1} at 950 °C. When the sweep gas is switched from helium to CO, the oxygen partial pressure gradient over the membrane becomes larger, and consequently the oxygen flux would increase significantly according to the Wagner equation.[45] Figure 6 shows the oxygen permeation performance of the SDC−LSF membranes with CO as the sweep gas. The oxygen permeation flux through the SDC70−LSF30 membrane increased to 8.92 × 10^{-7} mol·cm^{-2}·s^{-1} at 950 °C. The E_a values were estimated to be 96.5 ± 2.8, 96.2 ± 0.9, and 95.5 ± 2.0 kJ·mol^{-1} for SDC80−LSF20, SDC70−LSF30, and SDC60−LSF40, respectively. Obviously, all of the E_a values are reduced when CO is used as the sweep gas, which can be attributed to the enhanced surface exchange rate.[35]

Given that SDC70−LSF30 possesses the best performance, the stability of this membrane operating with three different sweep gases was performed, as shown in Figure 7. Over the whole test, the oxygen permeation flux of SDC70−LSF30 remained quite stable no matter what sweep gas was employed. Notably, the membrane exhibited perfect stability with CO_2 as the sweep gas and did not degrade at all after operating for about 150 h (kept a constant of 1.02 × 10^{-7} mol·cm^{-2}·s^{-1}). In contrast, oxygen permeation behavior completely disappeared for $Ba_{0.5}Sr_{0.5}Co_{0.8}Fe_{0.2}O_{3-\delta}$ when the sweep gas was switched to CO_2, although $Ba_{0.5}Sr_{0.5}Co_{0.8}Fe_{0.2}O_{3-\delta}$ exhibited very high oxygen permeation flux with helium as the sweep gas (Table 3). Compared to other cobalt-free dual-phase membranes under an air/CO_2 gradient (Table 3), SDC70−LSF30 also showed superior oxygen permeation flux. For a $Ce_{0.9}Pr_{0.1}O_{2-\delta}$−$Pr_{0.6}Sr_{0.4}FeO_{3-\delta}$ membrane with a thinner thickness of 0.6 mm, the flux was about 1.34 × 10^{-7} mol·cm^{-2}·s^{-1} at 950 °C.[25] As observed from the XRD pattern of the membrane surface exposed in the sweep gas (Figure 8a), one can see that there are only diffraction peaks corresponding to SDC and LSF without any other impurity phases, further confirming the good chemical stability of the membrane. Besides, LSF and SDC70−LSF30 powders also exhibit excellent chemical stability in CO_2. The phase structures are still well-kept even exposed in CO_2 at 900 °C for 12 h, as shown in Figure 8b. Moreover, the morphology of the post-tested membrane remains the same as that of the fresh one, as can be seen in Figure 9. LSF perovskite with less Sr^{2+} doped in the A site should be beneficial for maintaining the stability of $LaFeO_3$. Furthermore, the amount of the SDC phase is as much as 70 vol %, which would also prevent LSF from corrosion by CO_2, thereby leading to high chemical stability. All of the results prove that SDC70−LSF30 prepared by a one-pot combustion process is a chemically stable dual-phase ceramic membrane and has promising potential for oxygen separation and CO_2 capture.

4. CONCLUSION

In this work, cobalt-free SDC−LSF dual-phase ceramic oxygen permeation membranes were developed, and the oxygen permeation ability and durability of the membranes were investigated systematically. Ion interdiffusion behavior occurred between the fluorite phase SDC and perovskite phase LSF, and SDC was found to be codoped with samarium, lanthanum, and minor iron. SDC70−LSF30 (1.1 mm in thickness) possesses high oxygen permeation fluxes of 1.02 × 10^{-7} and 6.42 × 10^{-7} mol·cm^{-2}·s^{-1} at 900 °C with CO_2 and CO as the sweep gas, respectively. Moreover, the SDC70−LSF30 membrane showed excellent chemical stability and maintained a stable oxygen flux during a 450-h permeation test. The results demonstrate that SDC70−LSF30 is a promising CO_2-stable and reduction-tolerant membrane in oxygen separation and other related applications.

AUTHOR INFORMATION

Corresponding Author

*Tel: +86 551 63606929. Fax: +86 551 63602586. E-mail: wliu@ustc.edu.cn.

Notes

The authors declare no competing financial interest.

ACKNOWLEDGMENTS

This work was supported by the Ministry of Science and Technology of China (Grant 2012CB215403). The project was also supported by a research fund of the Key Laboratory for Advanced Technology in Environmental Protection of Jiangsu Province.

REFERENCES

(1) Luo, H.; Efimov, K.; Jiang, H.; Feldhoff, A.; Wang, H.; Caro, J. *Angew. Chem., Int. Ed.* **2011**, *50*, 759−763.
(2) Watenabe, K.; Yuasa, M.; Kida, T.; Teraoka, Y.; Yamazoe, N.; Shimanoe, K. *Adv. Mater.* **2010**, *22*, 2367−2370.
(3) Cheng, H.; Liu, J.; Lu, X.; Ding, W. *ACS Appl. Mater. Interfaces* **2011**, *3*, 4032−4039.
(4) Kniep, J.; Lin, Y. S. *Ind. Eng. Chem. Res.* **2011**, *50*, 7941−7948.
(5) Gong, Z.; Hong, L. *J. Membr. Sci.* **2011**, *380*, 81−86.
(6) Wang, H.; Werth, S.; Schiestel, T.; Caro, J. *Angew. Chem., Int. Ed.* **2005**, *44*, 6906−6909.
(7) Li, H.; Liu, Y.; Zhu, X.; Cong, Y.; Xu, S.; Xu, W.; Yang, W. *Sep. Purif. Technol.* **2013**, *114*, 31−37.
(8) Zhu, W.; Han, W.; Xiong, G.; Yang, W. *AIChE J.* **2008**, *54*, 242−248.
(9) Caro, J. *Chem. Ing. Tech.* **2006**, *78*, 899−912.
(10) Tan, X.; Liu, N.; Meng, B.; Sunarso, J.; Zhang, K.; Liu, S. *J. Membr. Sci.* **2012**, *389*, 216−212.
(11) Shao, Z. P.; Yang, W. S.; Cong, Y.; Dong, H.; Tong, J. H.; Xiong, G. X. *J. Membr. Sci.* **2000**, *172*, 177−188.
(12) Arnold, M.; Wang, H.; Feldhoff, A. *J. Membr. Sci.* **2007**, *293*, 44−52.
(13) Chen, W.; Chen, C.; Winnubst, L. *Solid State Ionics* **2011**, *196*, 30−33.
(14) Zhang, G.; Liu, Z.; Zhu, N.; Jiang, W.; Dong, X.; Jin, W. *J. Membr. Sci.* **2012**, *405*, 300−309.
(15) Efimov, K.; Klande, T.; Juditzki, N.; Feldhoff, A. *J. Membr. Sci.* **2012**, *389*, 205−215.
(16) Yi, J.; Zuo, Y.; Liu, W.; Winnubst, L.; Chen, C. *J. Membr. Sci.* **2006**, *280*, 849−855.
(17) Wang, B.; Yi, J.; Winnubst, L.; Chen, C. *J. Membr. Sci.* **2006**, *286*, 22−25.
(18) Yang, C.; Xu, Q.; Liu, C.; Liu, J.; Chen, C.; Liu, W. *Mater. Lett.* **2011**, *65*, 3365−3367.
(19) Liu, J.; Zhang, S.; Wang, W.; Gao, J.; Liu, W.; Chen, C. *J. Power Sources* **2012**, *217*, 287−290.
(20) Luo, Y.; Liu, T.; Gao, J.; Chen, C. *Mater. Lett.* **2012**, *86*, 5−8.
(21) Chen, T.; Zhao, H.; Xu, N.; Li, Y.; Lu, X.; Ding, W.; Li, F. *J. Membr. Sci.* **2011**, *370*, 158−165.
(22) Chen, T.; Zhao, H.; Xie, Z.; Feng, L.; Lu, X.; Ding, W.; Li, F. *Int. J. Hydrogen Energy* **2012**, *37*, 5277−5285.
(23) Choi, M. B.; Jeon, S. Y.; Hwang, H. J.; Park, J. Y.; Song, S. J. *Solid State Ionics* **2010**, *181*, 1680−1684.
(24) Li, Q.; Zhu, X.; He, Y.; Cong, Y.; Yang, W. *J. Membr. Sci* **2011**, *367*, 134−140.
(25) Luo, H.; Jiang, H.; Klande, T.; Cao, Z.; Liang, F.; Wang, H.; Caro, J. *Chem. Mater.* **2012**, *24*, 2148−2154.
(26) Zhu, X.; Li, M.; Liu, H.; Zhang, T.; Cong, Y.; Yang, W. *J. Membr. Sci.* **2012**, *394*, 120−130.
(27) Zhu, X.; Liu, H.; Cong, Y.; Yang, W. *Chem. Commun.* **2012**, *48*, 251−253.
(28) Huang, R.; Anderson, H. U. *J. Am. Ceram. Soc.* **1989**, *72*, 1382−1385.
(29) Huang, R.; Howng, W. Y. *J. Mater. Res.* **1996**, *11*, 3077−3082.
(30) Luo, H.; Jiang, H.; Efimov, K.; Liang, F.; Wang, H.; Caro, J. *Ind. Eng. Chem. Res.* **2011**, *50*, 13508−13517.
(31) Luo, H.; Jiang, H.; Klande, T.; Liang, F.; Cao, Z.; Wang, H.; Caro, J. *J. Membr. Sci.* **2012**, *423*, 450−458.
(32) Luo, H.; Jiang, H.; Efimov, K.; Caro, J.; Wang, H. *AIChE J.* **2011**, *57*, 2738−2745.
(33) Takamura, H.; Sugai, H.; Watanabe, M.; Kasahara, T.; Kamegawa, A.; Okada, M. *J. Electroceram.* **2006**, *17*, 741−748.
(34) Zhu, X.; Wang, H.; Yang, W. *J. Membr. Sci.* **2008**, *309*, 120−127.
(35) Zhu, X.; Li, Q.; He, Y.; Cong, Y.; Yang, W. *J. Membr. Sci.* **2010**, *360*, 454−460.
(36) Zhu, X.; Liu, H.; Li, Q.; Cong, Y.; Yang, W. *Solid State Ionics* **2011**, *185*, 27−31.
(37) Shannon, R. D. *Acta Crystallogr., Sect. A: Cryst. Phys., Diffr., Theor. Gen. Crystallogr.* **1976**, *32*, 751−767.
(38) Andersson, D. A.; Simak, S. I.; Skorodumova, N. V.; Abrikosov, I. A.; Johansson, B. *Proc. Natl. Acad. Sci. U.S.A.* **2006**, *103*, 3518−3521.
(39) Dudek, M. *Solid State Ionics* **2008**, *179*, 164−167.
(40) Sha, X.; Lv, Z.; Huang, X.; Miao, J.; Ding, Z.; Xin, X.; Su, W. *J. Alloys Compd.* **2007**, *428*, 59−64.
(41) Li, W.; Tian, T.; Shi, F.; Wang, Y.; Chen, C. *Ind. Eng. Chem. Res.* **2009**, *48*, 5789−5793.
(42) Khakpour, Z.; Yuzbashi, A.; Maghsodipour, A.; Ahmadi, K. *Solid State Ionics* **2012**, *227*, 80−85.
(43) Sanghavi, R.; Devanathan, R.; Nandasiri, M. I.; Kuchibhatla, S.; Kovarik, L.; Thevuthasan, S.; Prasad, S. *Solid State Ionics* **2011**, *204*, 13−19.
(44) Kosinski, M. R.; Baker, R. T. *J. Power Sources* **2011**, *196*, 2498−2512.
(45) Yang, C.; Xu, Q.; Liu, C.; Liu, J.; Chen, C.; Liu, W. *Mater. Lett.* **2011**, *65*, 3365−3367.
(46) Chen, C.; Burggraaf, A. J. *J. Appl. Electrochem.* **1999**, *29*, 355−360.
(47) Bouwmeester, H. J. M.; Burggraaf, A. J. In *Fundamentals of Inorganic Membrane Science and Technology*; Burggraaf, A. J., Cot, L., Eds.; Elsevier: Amsterdam, The Netherlands, 1996; pp 435−528.
(48) Elshof, J. E. T.; Bouwmeester, H. J. M.; Verweij, H. *Solid State Ionics* **1995**, *81*, 97−109.